Title
Polymer Directed Self-Assembly of pH-Responsive Antioxidant Nanoparticles

Journal
Langmuir, 31(12)

ISSN
0743-7463

Authors
Tang, Christina
Amin, Devang
Messersmith, Phillip B
et al.

Publication Date
2015-03-31

DOI
10.1021/acs.langmuir.5b00213

Peer reviewed

HHS Public Access

Author manuscript

Langmuir. Author manuscript; available in PMC 2016 March 31.

Published in final edited form as:

Langmuir. 2015 March 31; 31(12): 3612–3620. doi:10.1021/acs.langmuir.5b00213.

Polymer Directed Self-Assembly of pH-Responsive Antioxidant Nanoparticles

Christina Tang[1], **Devang Amin**[2], **Phillip B. Messersmith**[2,3], **John E. Anthony**[4], and **Robert K. Prud'homme**[1,1]

[1]Department of Chemical and Biological Engineering Princeton University Princeton, NJ 08544, United States

[2]Biomedical Engineering Department Northwestern University 2145 Sheridan Rd, Evanston, IL 60208 United States

[3]Departments of Bioengineering and Materials Science and Engineering University of California, Berkeley 210 Hearst Mining Building, Berkeley, CA 94720 United States

[4]Department of Chemistry University of Kentucky Lexington, KY 40506, United States

Abstract

We have developed pH-responsive, multifunctional nanoparticles based on encapsulation of an antioxidant, tannic acid (TA), using Flash NanoPrecipitation, a polymer directed self-assembly method. Formation of insoluble coordination complexes of tannic acid and iron during mixing drives nanoparticle assembly. Tuning the core material to polymer ratio, the size of the nanoparticles can be readily tuned between 50 and 265 nm. The resulting nanoparticle is pH-responsive, i.e. stable at pH 7.4 and soluble under acidic conditions due to the nature of the coordination complex. Further, the coordination complex can be coprecipitated with other hydrophobic materials such as therapeutics or imaging agents. For example, coprecipitation with a hydrophobic fluorescent dye creates fluorescent nanoparticles. *In vitro*, the nanoparticles have low cytotoxicity show antioxidant activity. Therefore, these particles may facilitate intracellular delivery of antioxidants.

1. Introduction

Multifunctional nanoparticles are promising for biomedical applications such as multimodal imaging, theragnostics and image-guided therapies.[1-6] Multifunctional polymeric nanoparticles are especially promising for delivery platforms because they are stable *in vivo* and *in vitro*, can encapsulate a variety of drugs, and provide release over prolonged

[1]Corresponding author: prudhomm@princeton.edu; ph: 609-258-4577 .

Supporting Information

Nanoparticle size distributions of nanoparticles produced at pHs between 2 and 7.4, 1-HNMR of tannic acid and iron nanoparticles, effect of total solids concentration on nanoparticle size distribution, summary of nanoparticle formulations, tannic acid and iron nanoparticle size distributions before and after dialysis, optical properties of nanoparticle dispersions as a function of pH, effect of nanoparticles on cell viability, confocal microscopy images as a function of depth, antioxidant activity assays for tannic acid nanoparticles, ascorbic acid and tannic acid, and expanded methods regarding cell studies. This material is available free of charge via the Internet at http://pubs.acs.org.

periods.[6-8] Coating the nanoparticles with a hydrophilic polymer brush, e.g. polyethylene glycol (PEG) prolongs circulation time and avoids clearance by the mononuclear phagocytic system.[4, 6-7, 9] The surface of the nanoparticles can be further modified with targeting ligand(s).[6, 9]

Preparation of polymer nanoparticles via bottom-up, precipitation methods allows for high core loadings and the inclusion of multiple components in the nanoparticle core.[10-11] Flash NanoPrecipitation (FNP) is a rapid and scalable nanoparticle (50-500 nm) production method that leverages the advantages of bottom-up precipitation methods with uniformity dictated by micellization of self-assembled block copolymers to encapsulate desired cargo.[9, 12] In FNP, an amphiphilic block copolymer is dissolved in organic solvent with a desired core material, such as therapeutic and/or imaging agent, and is rapidly mixed against a miscible anti-solvent to induce rapid precipitation of the core materials and the hydrophobic block of the block copolymer.[13-14] The self-assembly of the amphiphilic block copolymer directs nanoparticle assembly with relatively narrow size distributions. Precipitation of the core material is arrested by adsorption of the hydrophobic block of the block copolymer while the hydrophilic block sterically stabilizes the nanoparticle. Therefore, given sufficient affinity between the hydrophobic block of the amphiphilic block copolymer and the core material, production of uniform particles requires the rate of amphiphilic block copolymer self-assembly be matched with the rate of nucleation and growth of the precipitating core materials[15]. Once assembled, the nanoparticles are kinetically frozen and there is no dynamic exchange of the individual block copolymer chains.[16] Further, FNP is a convenient platform to tailor the surface chemistry of nanoparticles as PEG-based functionalized block copolymers can be incorporated during the mixing process. These functionalized block copolymers facilitate conjugation to a range of ligands to enable targeted delivery of the nanoparticle.[17-19]

There are several examples of using FNP to encapsulate hydrophobic functional materials including therapeutics and/or imaging agents. For example, Gindy et al. produced multicomponent nanoparticles containing hydrophobic colloidal gold (~5 nm modified with dodecanethiol) as an illustrative imaging agent and β-carotene as a model therapeutic using PEG-*b*-polycaprolactone for stabilization.[19] In another example, Shan et al. used FNP to co-localize upconverting nanophosphors with meso-tetraphenyl porphine, a photosensitizer, within a 100 nm particle stabilized by PEG-*b*-polylactic acid for photodynamic therapy.[20] However, the technique has thus far been limited to the encapsulation of hydrophobic materials; an *n*-octanol/water partition coefficient (logP) greater than 6 is preferred to achieve sufficient supersaturation and ensure stable nanoparticles.[21-22]

Extending FNP to water soluble species would enable applications in the delivery of peptides, antioxidants and other molecules that have tremendous therapeutic potential. In this work, we focus on the encapsulation of antioxidants, natural scavengers of reactive oxygen species, for potential treatment of many diseases including cardiovascular diseases such as atherosclerosis, and neurological disorders including Alzheimer's.[23-26] Formulating the antioxidants into nanoparticles using FNP may be advantageous as high loadings of therapeutics and targeted delivery are possible.

Tannic acid is a high molecular weight, polyphenolic compound with demonstrated antioxidant activity.[27-30] While its intrinsic water solubility is too high to enable direct precipitation into nanoparticles using FNP, we have previously demonstrated that ion-pairing can reduce the solubility of compounds to enable encapsulation by FNP.[31] Caruso and co-workers have recently demonstrated that coordination complexes of iron and tannic acid can form insoluble thin films and capsules.[32] Combinations of metal and polyphenols have also been used to synthesize hydrogels and coatings.[33-34] TA based coatings were found to have antibacterial properties, be resistant to fouling by bacterial and mammalian cells, and able to scavenge radical and non-radical reactive oxygen species.[34] Using these concepts, we encapsulated tannic acid using FNP by forming coordination complexes with iron during the mixing and assembly process. Our goal is to maximize the delivery of the antioxidant so formation of a dense core of TA:Fe complex is desired rather than surface films, capsules, or hydrogels that have been accomplished previously.[32-34] *A priori* with was not clear that the coordination complexation would be rapid enough to enable encapsulation of the water soluble TA. The effects of formulation parameters such as relative concentrations of tannic acid and iron ([TA:Fe]) as well as of block copolymer to tannic acid-iron complex [PS-b-PEG:TA-Fe] on nanoparticle assembly are explored. We further coprecipitated the tannic-acid iron complex with a hydrophobic fluorescent dye to demonstrate the ability to produce multifunctional nanoparticles with therapeutic and imaging functionalities. The antioxidant activity of the nanoparticles *in vitro* is evaluated.

2. Experimental Section

2.1 Materials

ACS grade tannic acid and iron (III) chloride hexahydrate were purchased from Sigma Aldrich. HPLC grade solvents: acetone, tertrahydrofuran (THF) and dimethyl sulfoxide (DMSO) were obtained from Fisher Scientific. Phosphate buffered saline without Ca^{2+} and Mg^{2+} was obtained from Lonza. Water (MQ) was purified by 0.2 μm filtration and four stage deionization to a resistivity of 17 MΩ or greater (NANOpure Diamond, Barnstead International, Dubuque, IA). Block copolymer, polystyrene 1.6 kDa -b- polyethylene oxide 5kDa (PS-b-PEG), was from Polymer Source (Dorval, QC, CAN). All materials were used as received. EtTP-5 was synthesized as previously described.[35]

2.2 Nanoparticle Assembly

FNP was performed using a hand operated confined impinging jet mixer with dilution as previously described.[36] Mixing was performed manually with a confined impinging jet mixer and 1 mL syringes (National Scientific) as previously described achieving mixing Reynolds number of Re ~ 1300.[14, 17] Typically, the block copolymer and tannic acid were dissolved in a water miscible organic solvent (i.e. THF, acetone, or DMSO) at 10 mg/mL and 4 mg/mL, respectively. The components in the organic solvent (0.5 mL) were rapidly mixed against 0.5 mL of an aqueous stream of $FeCl_3$ (1 mg/mL) dissolved in water or buffer and collected in a 4 mL bath of PBS to quench nanoparticle rearrangement. The final organic solvent concentration was 10% by volume. To remove the organic solvent, the resulting nanoparticle dispersions were placed in regenerated cellulose tubing with a molecular weight cutoff of 6-8 kDa (Spectra/Por, Spectrum Laboratories, USA) and

dialyzed against a 100-fold volume of water or buffer bath for 24 hours with 4 changes of the bath.

2.3 Nanoparticle Characterization

Nanoparticle size distributions were measured after mixing and after dialysis by dynamic light scattering using a Zetasizer Nano-ZS (Malvern Instruments, Malvern, UK) with a backscatter detection angle of 173°. Distributions are reported using the normal resolution mode intensity weighted distribution (average of 4 measurements). DLS was used to determine if the resulting nanoparticles were uniform which we define as a nanoparticle size distribution with a single Gaussian peak. For samples with a nanoparticle size distribution with a single Gaussian peak, the reported size is the Peak 1 Mean Intensity. The PDI is a measure of the breadth of the particle distribution defined from the moments of the cumulant fit of the autocorrelation function calculated by the instrument software which is appropriate for samples with PDI < 0.3.[37] Samples for TEM were prepared by placing 5 μL of the nanoparticle dispersion on an Ultrathin Carbon Film on a Holey Carbon Support film on 400 mesh copper grid (Ted Pella, Inc., Redding, CA) and drying under ambient conditions. The samples were imaged using a Philips CM100 TEM (Eindhoven, The Netherlands) operated at an accelerating voltage of 100 kV. UV absorbance spectra of the nanoparticle dispersions were collected at room temperature with an Evolution 300 UV-visible spectrophotometer (Thermo Electron Corporation, Madison, WI, USA). Absorbance at wavelengths between 450 and 800 nm were recorded. Nanoparticle dispersions were diluted to below 1 μg/mL of total dye in suspension in order to minimize light scattering effects on fluorescence in intensity measurements after mixing and after dialysis as previously described.[38] Emission spectra (500 to 800 nm) of the nanoparticle dispersions were measured with an excitation wavelength of 460 nm excitation and emission slit widths of 5 nm, PMT voltage at 400 V, and 90° angle arrangement of incident and detector using a Hitachi F-7000 Fluorescence Spectrophotometer, Hitachi High Technologies, Tokyo, Japan). The solvent of the nanoparticle dispersions was switched from water to D_2O for NMR analysis with Amicon Ultra-2 Centrifugal devices with a 50 kDa molecular weight cutoff (Millipore, Billerica, MA) according to the manufacturer's specifications. ^1H nuclear magnetic resonance (^1H NMR) spectra were recorded in D_2O with 4,4-dimethyl-4-silapentane-1-sulfonic acid DSS as an internal standard (Cambridge Isotopes, Tewksbury, MA) using a Bruker Avance-III 500 MHz (Bruker Biosciences, Inc. Billerica, MA). Nanoparticle stability was assessed by monitoring the nanoparticle size distributions by Dynamic Light Scattering as well as the optical properties by UV spectroscopy as a function of time after mixing.

2.4 *In vitro* Analysis

Confluent NIH 3T3 fibroblasts (ATCC, Manassas, VA) were treated with sterile-filtered TA NPs (d = 79 ± 2 nm, 1.5 wt% iron) for 24 hours, after which cell viability was measured using a 3-hour neutral red uptake assay.[39] Antioxidant activity was measured with a dichlorofluorescein assay.[40] Briefly, 40,000 cells/well were plated on a 96-well plate, grown for 24 hours, and treated with 2′, 7′-dichlorofluorescein diacetate (DCFH-DA, Sigma-Aldrich, St. Louis, MO) for 1 hour. After the DCFH-DA was removed, 600 μM 2, 2′-azo-bisamidinopropane (ABAP, Sigma-Aldrich) and 50 μg/mL TA NPs (d = 79 ± 2 nm, 1.5 wt% iron) were added. The fluorescence due to the intracellular oxidization of the non-

fluorescent probe to fluorescent dichlorofluorescein (λ_{ex} = 485 nm and λ_{em} = 500 nm) as a result of the oxidative stress was monitored for 90 minutes using a Molecular Devices Gemini EM Fluorescence/Chemiluminescence Plate Reader (Keck Biophysics, Northwestern University). Both the neutral red uptake and DCF assays were performed in triplicate. Nanoparticle uptake was monitored by confocal microscopy. Cells were seeded, grown for 24 hours, and treated with 100 ug/mL TA NPs (d = 73.5 ± 1.5 nm, 1.5 wt% iron, 2.3 wt% EtTP-5) for 24 hours. The treated cells were then rinsed and stained with LysoTracker Green® DND-26 and Hoechst 33258 (Life Technologies, Grand Island, NY) to visualize the lysosome and nucleus, respectively. Imaging was performed using an Inverted Zeiss Axio Observer Z1 confocal microscope (QBIC, Northwestern University) and colocalization of lysosomes and nanoparticles was quantified with the Manders overlap coefficient computed using the Zen 2009 image processing program (Zeiss).[41-42] Further details are included in the Supporting Information.

3. Results and Discussion

3.1 Nanoparticle Assembly and Characterization

Formulation of Tannic Acid—FNP was performed with TA and a PEG-based amphiphilic block copolymer (polystyrene (1.6 kDa)-b-polyethylene glycol (5 kDa), PS-b-PEG) dissolved in acetone and mixed against an aqueous stream. Nanoparticles could be formed initially at a range of pHs (from pH 2 to pH 7.4) (Supporting Information Figure S. 1). However, using PBS at pH 7.4 resulted in unstable particles when dialyzed against PBS with a pH of 7.4 or against DI water. The nanoparticles made at pH 2 and in water were initially 84 ± 3 nm. While stable in the mixed solvent, the particle size swelled upon dialysis against water to 129 ± 3 nm. Macroscopic precipitates formed within 24 hours of storage at 4°C or at room temperature. Precipitates likely arise from the process of solubilization of TA from the core and complexation of TA and PEG[43] (the water soluble portion of the block copolymer). Therefore, the TA alone is not sufficiently hydrophobic for encapsulation by FNP.

Formulation of Tannic Acid/Iron Complexes—In order to encapsulate the TA within the core of the nanoparticles using FNP, we explored encapsulating coordination complexes of tannic acid and metal salts. Since TA is known to form insoluble complexes with ferric iron and the complexes have been well characterized,[32, 44-45] we aimed to complex and encapsulate the TA and ferric iron coordination complex during mixing. This approach requires that (1) the TA/iron complex occurs sufficiently fast to enable encapsulation during mixing and (2) the complex is sufficiently hydrophobic to form a stable nanoparticle.

The nature and solubility of the TA/iron complex has been studied previously.[32, 44-45] The Fe(III) complexes with the gallate ligand of tannic acid and the number of coordinating ligands varies with pH. At acidic pH, the mono-complex is formed and is soluble whereas at basic pH, the tris-complex is formed and is insoluble. We performed FNP by mixing TA and PS-b-PEG dissolved in acetone in one stream and iron (III) chloride dissolved in PBS at pH 7.4 in a second stream. The mixture was quenched with a bath of PBS, pH 7.4, conditions under which the complex is expected to be insoluble. The initial concentrations of iron

relative to tannic acid (excess iron) were based on previous reports of assembly of TA/iron coordination complexes and included in the Supporting Information (Table S.1).[32] Upon mixing, we observed instantaneous formation of macroscopic, dark purple precipitates. This dark precipitate is consistent with insoluble, amorphous iron tannates that form due to colloidal associations of TA with ferric hydroxide.[46] This result indicates the rate of complex formation is sufficiently fast for encapsulation using FNP. However, the rate of precipitation was fast relative to self-assembly of the amphiphilic block copolymer and large (macroscopic) precipitates formed.

In order to successfully encapsulate the TA/iron complexes within the core of nanoparticles, the rate of self-assembly must be balanced with the rate of complexation and subsequent precipitation. Using a 2 to 1 weight ratio of block copolymer to total tannic acid and iron [PS-b-PEG:TA-Fe] and an excess of iron (1.6 molar equivalents of TA molecules), we were able to produce homogeneous dispersions of TA/iron complexes (Figure 1). The dispersions appeared red which is consistent with the tris-complex of TA and iron expected at pH 7.4.[32, 45] The nanoparticle size is 52 ± 1 nm with a PDI of 0.20 as measured by DLS (reported intensity average) (Figure 2) and is consistent with TEM analysis (Figure 1). Evidence of a soluble PEG coating on the nanoparticles is evident by ^{1}H-NMR analysis of the nanoparticles dispersed in D_2O (Supporting Information Figure S.2). If FNP is performed without the block copolymer, macroscopic aggregation of the TA/iron complex is observed within minutes (Figure 1). Combined, these results indicate that the TA/iron core is stabilized by the amphiphilic block copolymer.

The nanoparticle assembly kinetics and resulting size distribution are affected by the iron concentration relative to tannic acid. Uniform particles 52 ± 1 nm in diameter were obtained using 1.6 molar equivalents of iron to tannic acid (Figure 2). At lower iron concentrations, the nanoparticle dispersions appear red (tris-complex of TA and iron), but the intensity weighted distribution shows evidence of two size populations of diameter ~30 nm or ~400 nm (Figure 2). This result suggests that at lower iron concentrations the rate of complexation is slow relative to micellization of the block copolymer. This mismatch in time scales results in the block copolymer rapidly forming micelles[47] and on a longer time scale stabilizing the TA-Fe complex. The increase in nanoparticle size (400 nm compared to 50 nm) occurs because the steric stabilizing polymer was depleted by the formation of empty micelles and results in the bimodal distribution seen in Figure 2. As the relative iron concentration is increased to 3.1 molar equivalents of iron relative to TA, the color of the nanoparticle dispersion changes to a dark purple (TA/iron precipitates[46, 48-49]). The ferric tannate precipitates have aggregated into nanoparticles stabilized by the block copolymer (~200 nm by DLS). Again, there is a micelle peak in the intensity weighted size distribution (peak at ~30 nm[15]) (Figure 2) due to empty polymer micelles in addition to the desired TA-Fe nanoparticles. However, we believe the mechanism is different. At the higher iron concentration (3.1 molar equivalents of iron), the presence of micelles is likely due to limited affinity between the polystyrene (the hydrophobic portion of the amphiphilic block copolymer) and the more polar, non-stoichiometric TA/Fe precipitate with excess cationic charge.[46, 48-49] When there is little affinity between the hydrophobic block and the core material, larger nanoparticles and empty micelles are produced.[50-51]

3.1.1 Tuning Nanoparticle Size

Effect of Solute Concentration: Since formulation of uniform nanoparticles encapsulating the tris-complex of TA and iron using FNP was possible using 1.6 molar equivalents of iron, we examined tuning the size of the resulting nanoparticles. Increasing the total solids concentration from 1.5 mg/mL to 3 mg/mL led to an increase in particle size from 52 ± 1 nm (PDI 0.20) to 79 ± 2 nm (PDI 0.23) (Figure 3a). However, using acetone as the organic solvent, the total solids concentration that could be used while still producing a unimodal nanoparticle size was 3 mg/mL (in the final nanoparticle dispersion). With acetone, concentrations above 3 mg/mL resulted in a micelle population (Supporting Information Figure S.3). To further increase the nanoparticle size, the total solids concentration was increased to 6 mg/mL (in the final nanoparticle dispersion) using DMSO as the organic solvent and a nanoparticle size of 114 ± 3 nm (PDI 0.25) was achieved. Supersaturation of tannic acid and polystyrene block which dictates the nucleation rate and self-assembly rate, respectively, are more appropriately matched at high concentrations using DMSO to produce nanoparticles with a narrow size distribution.

Effect of Stabilizing Block Copolymer to Core Ratio: Since nanoparticle assembly of hydrophobic compounds is governed by the relative rates of self-assembly of the amphiphilic block copolymer and precipitation of the core materials, nanoparticle size can also be tuned by manipulating the relative concentration of block copolymer to core material. Using acetone, there was a small window of PS-b-PEG to [TA:Fe] ratios appropriate for making uniform particles; ratios below 1.5:1 resulted in macroscopic precipitates. The macroscopic precipitation at reduced PS-b-PEG concentrations occurs because there is a mismatch in the rate of complexation and precipitation and micellization and the amount of PS-b-PEG that adsorbs to the growing insoluble complex is not sufficient for stabilization. Changing the organic solvent to THF in which both polystyrene and PEG are soluble, the ratio of PS-b-PEG to [TA-Fe] from 2:1 to 1:1 produced uniform particle size distributions (Figure 3b). The rates of PS-b-PEG self-assembly and complexation of TA:Fe from THF are better matched than in acetone at the range of block copolymer ratios to core material ratios tested. The size of the particle increased from 86 ± 2 nm to 266 ± 20 nm by decreasing the ratio of PS-b-PEG to [TA-Fe] from 2:1 to 1:1 by weight. The decrease in PS-b-PEG concentration relative to [TA-Fe] decreases the rate of polymer self-assembly (i.e. the rate of steric stabilization) relative to the rate of particle growth; therefore, the resulting nanoparticles are larger.

Given an appropriate choice of the organic solvent to match the relative solubilities of the polystyrene block of the amphiphilic block copolymer and TA-iron complex, the nanoparticle size could be tuned between ~ 50 and 265 nm. A table summarizing the formulations is provided in the Supporting Information (Table S.1).

3.1.2 Nanoparticle Stability—Another important consideration in formulating the antioxidant-loaded nanoparticles is stability of the nanoparticle over time. Processes such as Ostwald ripening,[22] recrystallization,[31] or particle aggregation[51] may occur if the TA-iron coordination complex is too labile. During dialysis against PBS to remove the residual organic solvent, the particle size was stable (Supporting Information Figure S.4). The

particle sizes were constant for at least one month when the particles were stored in PBS at room temperature (Figure 4a). Further, after a month of storage the nanoparticle dispersions appear red with the maximum UV absorbance at 496 nm (Figure 4b) which is consistent with the tris-complex of tannic acid[32, 45] and iron initially encapsulated. Reduction of ferric (Fe^{3+}) to ferrous (Fe^{2+}) iron upon binding with the gallate ligand is possible.[52] However, under the conditions used i.e. presence of phosphate buffer at basic pH and excess iron, the reduction of Fe^{3+} is inhibited and autooxidation of Fe^{2+} is expected, both favoring the ferric iron oxidation state.[52-53] Additionally, polyphenols such as TA strongly stabilize Fe^{3+}, a hard Lewis acid, over Fe^{2+}, only a marginal Lewis acid, due to hard metal ion interactions with the deprotonated polyphenol ligands that behave as hard Lewis bases.[52] Therefore, the FNP process stabilizes nanoparticles encapsulating octahedral tris TA-Fe^{3+} complexes.

3.1.3 Effect of pH on Nanoparticle—Because the TA/iron complex is affected by pH, we compared the properties of the nanoparticle dispersions at pH 7.4 (as made) and when dialyzed against water resulting in a nanoparticle dispersion at pH 5. At basic pH the octahedral tris(tannic acid) complex appears red in color[32, 45]. When the pH is shifted to 5, dynamic light scattering shows a relatively small change in the size distribution; a shoulder at smaller sizes is seen in Figure 5 at pH 5 that is not evident at pH 7.4. The pH decrease from 7 to 5 causes the dispersion to change from red to purple (maximum absorbance at 561 nm) as shown in Figure 5, which is consistent with the bis-complex of tannic acid and iron expected at pHs between 3 and 6.[32, 45] At pH 5, iron is bound by two gallate ligands producing a blue-purple Fe^{3+} complex due to their ligand-to-metal charge transfer bands.[32, 52] This color change is reversible (Figure S.5).

TEM shows a change in nanoparticle structure upon changing the pH. At pH 7.4, the nanoparticles have a homogenous solid spherical core containing iron encapsulated within a block copolymer shell (Figure 5). However at pH 5, the core of the particles have swollen and appear porous under TEM due to solubilization of a portion of the TA-iron complex. Further, in the TEM micrograph a portion of the block copolymer appears drawn away from the surface of the nanoparticle as long filaments. The stability constant of TA-iron bis-complex at pH 5 is ~10^9 compared to ~10^{17} for the tris-complex[45] possibly leading to some degree of nanoparticle disassembly and rearrangement.

3.2 Multifunctional Nanoparticles

The calculated hydrophobicity of TA is logP 6.2 (Molinspiration[54]) roughly the same hydrophobicity (logP) of 1-tetradecanol. Therefore, it is reasonable to expect that hydrophobic organic species could be coprecipitated with the TA/iron coordination complex. For example, we have previously encapsulated a hydrophobic fluorescent dye, EtTP-5 for confocal imaging.[17, 38] Performing FNP of 2:1 PS-b-PEG to [TA-Fe] by weight and 1.6 molar equivalents of iron to tannic acid with the addition of EtTP-5 in the organic stream (THF), nanoparticles with a narrow size distribution of 72 ± 1 nm and PDI of 0.23 were obtained (Figure 6a). After dialysis and passing through a 0.45 micron nylon syringe filter, the resulting size was 73 ± 2 nm (PDI 0.21). The size of the nanoparticles containing EtTP-5 was comparable to particles made under the same conditions without EtTP-5 (80 nm ± 2 nm, PDI 0.20 i.e. within 10% and within experimental error). Since the EtTP-5 loading

was 1 wt.% of the nanoparticle core, the size of the nanoparticle was not expected to be significantly affected by the addition of the EtTP-5. Measurements of UV absorbance of the nanoparticle dispersion show peaks associated with the TA/iron complex as well as the EtTP-5 (Figure 6b). The nanoparticles are fluorescent (EtTP-5 excitation at 460 nm and emission at 635 nm and 695 nm). The ratio of the intensity of the peak at 635 nm to the peak at 695 nm (Figure 6c) is consistent with the dye dispersed in the hydrophobic core of the nanoparticle as has been observed the case of EtTP-5 dispersed in the core of a polystyrene nanoparticle.[38] Based on this result and previous results with EtTP-5 dispersed in the hydrophobic nanoparticle core, EtTP-5 does not partition out of the nanoparticle core and can be used to track nanoparticles using confocal microscopy.[17, 38] This result serves as an example of how the coordination complexes of TA and iron can be coprecipitated with other functional hydrophobic compounds or therapeutics to achieve multifunctional nanoparticles. Here, we have produced a fluorescent, pH-responsive, antioxidant containing nanoparticle.

3.3 *In Vitro* Antioxidant Activity and Uptake

We explored the intracellular antioxidant activity of the TA-loaded nanoparticles using 3T3 fibroblasts. When cells were treated with increasing concentrations of TA-loaded nanoparticles for 24 hours, cell viability was over 70% for concentrations up to 100 μg/mL (Supporting Information Figure S.6) demonstrating the low cytotoxicity of the nanoparticles.

Antioxidant activity was monitored using a dichlorofluorescein (DCF) assay[40] in which non-fluorescent dichlorofluorescein diacetate probe (DCFH-DA) is deacetylated by intracellular esterases and subsequently oxidized to fluorescent dichlorofluorescein (DCF) in the presence of peroxyl radicals generated by 2, 2′-azo-bis-amidinopropane (ABAP) (Figure 7a). In the presence of the 50 μg/mL TA-loaded nanoparticles, the ABAP induced production of DCF was reduced by approximately 3-fold compared to untreated cells after 90 minutes (Figure 7b). At TA-loaded nanoparticle concentrations greater than 20 μg/mL, antioxidant activity was comparable to tannic acid and ascorbic acid (vitamin C) at the same concentration (Supporting Information Figure S.8). This result demonstrates the antioxidant activity of the TA-loaded nanoparticles. Cells were incubated with 1000 μg/mL of nanoparticles containing TA and EtTP-5 (red) for 24 hours. To assess whether TA NPs entered acidic lysosomes, these cells were counterstained with LysoTracker Green®. Confocal microscopy suggests that the TA NPs were internalized and co-localized with lysosomes (Figure 7c). This observation was quantitatively verified by a Manders overlap coefficient of 0.76 between the EtTP-5 and LysoTracker Green® channels computed using the Zen 2009 image processing program (Zeiss) and a Manders coefficient above 0.6 indicates colocalization.[41-42] TA NP internalization was further confirmed via z-stack imaging, as shown in Supporting Information Figure S.6. Given the slightly acidic pH (4.5-5) of the lysosome[55] and the transition from the stable tris-complex of TA and Fe^{3+} to less stable bis-complex below pH 6,[32] these particles may release TA in the lysosome, potentially providing a valuable platform for intracellular delivery of antioxidants with potential applications in preventing cellular injury and death due to excess reactive oxygen species implicated in cardiac diseases.[25] This is the focus of ongoing studies. The fact that TA nanoparticles are equally effective as free, unencapsulated TA demonstrates the promise of this approach. We have selected PS-b-PEG as a model system to examine the self-

assembly of the precipitating coordination complexes in the presence of an amphiphilic block copolymer. In future work, the use of biodegradable hydrophobic blocks such as PLA-b-PEG will be explored as has been explored in previous studies.[56]

4. Conclusions

Multifunctional, pH responsive nanoparticles that encapsulate antioxidant-metal coordination complexes can be produced using FNP, a polymer-directed self-assembly method. We encapsulated the tannic acid antioxidant by forming insoluble coordination complexes with Fe^{3+} during the mixing and assembly process. The tris-complex of tannic acid and iron forms sufficiently rapidly to be encapsulated within the core of the nanoparticle and effectively stabilizes the nanoparticle. Once formed the TA-Fe nanoparticles are stable for at least a month. The size of the nanoparticles can be tuned between 50 and 265 nm and can be coprecipitated with other hydrophobic moieties of interest e.g. therapeutics, dyes, etc. *In vitro* the nanoparticles show low cytotoxicity, are internalized in the lysosome of 3T3 fibroblasts and show antioxidant activity. Based on the pH of the lysosome and pH responsive nature of the TA/iron complex, these particles may be valuable platform for intracellular delivery of antioxidants with potential applications in preventing cellular injury and death due to excess reactive oxygen species implicated in cardiac diseases.

Supplementary Material

Refer to Web version on PubMed Central for supplementary material.

Acknowledgements

This work was supported by Princeton University's Intellectual Property Accelerator Program and in part by National Institutes of Health grant R01 DE014193 to PBM. DA was supported in part by NIH Predoctoral Biotechnology Training Grant T32GM008449. We acknowledge insights on the mysteries of inorganic ligand chemistry supplied by Prof. Andrew Bocarsly of the Princeton Department of Chemistry.

References

(1). Lee D-E, Koo H, Sun I-C, Ryu JH, Kim K, Kwon IC. Multifunctional nanoparticles for multimodal imaging and theragnosis. Chem. Soc. Rev. 2012; 41:2656–2672. [PubMed: 22189429]

(2). Jia F, Liu X, Li L, Mallapragada S, Narasimhan B, Wang Q. Multifunctional nanoparticles for targeted delivery of immune activating and cancer therapeutic agents. J. Control. Release. 2013; 172:1020–1034. [PubMed: 24140748]

(3). Alexis, F.; Pridgen, EM.; Langer, R.; Farokhzad, OC. Drug Delivery. Springer; 2010. Nanoparticle technologies for cancer therapy; p. 55-86.

(4). Torchilin VP. Multifunctional nanocarriers. Adv. Drug Deliver. Rev. 2012; 64:302–315.

(5). Petros RA, DeSimone JM. Strategies in the design of nanoparticles for therapeutic applications. Nat. Rev. Drug Discov. 2010; 9:615–627. [PubMed: 20616808]

(6). Bao G, Mitragotri S, Tong S. Multifunctional nanoparticles for drug delivery and molecular imaging. Annu. Rev. Biomed.Eng. 2013; 15:253–282. [PubMed: 23642243]

(7). Levine DH, Ghoroghchian PP, Freudenberg J, Zhang G, Therien MJ, Greene MI, Hammer DA, Murali R. Polymersomes: a new multi-functional tool for cancer diagnosis and therapy. Methods. 2008; 46:25–32. [PubMed: 18572025]

(8). Elsabahy M, Wooley KL. Design of polymeric nanoparticles for biomedical delivery applications. Chem. Soc. Rev. 2012; 41:2545–2561. [PubMed: 22334259]

(9). Tyrrell ZL, Shen Y, Radosz M. Fabrication of micellar nanoparticles for drug delivery through the self-assembly of block copolymers. Prog. Polym. Sci. 2010; 35:1128–1143.

(10). Rowe, JM.; Johnston, KP. Formulating Poorly Water Soluble Drugs. Springer; 2012. Precipitation Technologies for Nanoparticle Production; p. 501-568.

(11). Lepeltier E, Bourgaux C, Couvreur P. Nanoprecipitation and the “Ouzo effect”: Application to drug delivery devices. Adv. Drug Deliver. Rev. 2014; 71:86–97.

(12). Hayward RC, Pochan DJ. Tailored assemblies of block copolymers in solution: it is all about the process. Macromolecules. 2010; 43:3577–3584.

(13). Gindy ME, Panagiotopoulos AZ, Prud'homme RK. Composite block copolymer stabilized nanoparticles: simultaneous encapsulation of organic actives and inorganic nanostructures. Langmuir. 2008; 24:83–90. [PubMed: 18044945]

(14). Johnson BK, Prud'homme RK. Chemical processing and micromixing in confined impinging jets. AlChE J. 2003; 49:2264–2282.

(15). Johnson BK, Prud'homme RK. Flash nanoprecipitation of organic actives and block copolymers using a confined impinging jets mixer. Aust. J. Chem. 2003; 56:1021–1024.

(16). Choi S-H, Bates FS, Lodge TP. Molecular Exchange in Ordered Diblock Copolymer Micelles. Macromolecules. 2011; 44:3594–3604.

(17). D'Addio SM, Baldassano S, Shi L, Cheung L, Adamson DH, Bruzek M, Anthony JE, Laskin DL, Sinko PJ, Prud'homme RK. Optimization of cell receptor-specific targeting through multivalent surface decoration of polymeric nanocarriers. J. Control. Release. 2013; 168:41–49. [PubMed: 23419950]

(18). Ji S, Zhu Z, Hoye TR, Macosko CW. Maleimide Functionalized Poly (ε-caprolactone)-block-poly (ethylene glycol)(PCL-PEG-MAL): Synthesis, Nanoparticle Formation, and Thiol Conjugation. Macromol. Chem. Phys. 2009; 210:823–831. [PubMed: 21731402]

(19). Gindy ME, Ji S, Hoye TR, Panagiotopoulos AZ, Prud’homme RK. Preparation of poly (ethylene glycol) protected nanoparticles with variable bioconjugate ligand density. Biomacromolecules. 2008; 9:2705–2711. [PubMed: 18759476]

(20). Shan J, Budijono SJ, Hu G, Yao N, Kang Y, Ju Y, Prud'homme RK. Pegylated Composite Nanoparticles Containing Upconverting Phosphors and meso-Tetraphenyl porphine (TPP) for Photodynamic Therapy. Adv. Funct. Mater. 2011; 21:2488–2495.

(21). Zhu Z. Flash Nanoprecipitation: Prediction and Enhancement of Particle Stability via Drug Structure. Mol. Pharm. 2014; 11:776–786. [PubMed: 24484077]

(22). Pustulka KM, Wohl AR, Lee HS, Michel AR, Han J, Hoye TR, McCormick AV, Panyam J, Macosko CW. Flash nanoprecipitation: Particle structure and stability. Mol. Pharm. 2013; 10:4367–4377. [PubMed: 24053447]

(23). Persson T, Popescu BO, Cedazo-Minguez A. Oxidative Stress in Alzheimer’s Disease: Why Did Antioxidant Therapy Fail? Oxid. Med. Cell Longev. 2014; 2014

(24). Stanton RC. Oxidative stress and diabetic kidney disease. Current diabetes reports. 2011; 11:330–336. [PubMed: 21557044]

(25). Farbstein D, Kozak-Blickstein A, Levy AP. Antioxidant vitamins and their use in preventing cardiovascular disease. Molecules. 2010; 15:8098–8110. [PubMed: 21063272]

(26). Wood LG, Wark PA, Garg ML. Antioxidant and anti-inflammatory effects of resveratrol in airway disease. Antioxid. Redox Sign. 2010; 13:1535–1548.

(27). Gülçin İ, Huyut Z, Elmastaş M, Aboul-Enein HY. Radical scavenging and antioxidant activity of tannic acid. Arab. J. Chem. 2010; 3:43–53.

(28). Andrade RG Jr, Ginani JS, Lopes GK, Dutra F, Alonso A, Hermes-Lima M. Tannic acid inhibits in vitro iron-dependent free radical formation. Biochimie. 2006; 88:1287–1296. [PubMed: 16600466]

(29). Khan NS, Ahmad A, Hadi S. Anti-oxidant, pro-oxidant properties of tannic acid and its binding to DNA. Chem. Biol. Interact. 2000; 125:177–189. [PubMed: 10731518]

(30). Hagerman AE, Riedl KM, Jones GA, Sovik KN, Ritchard NT, Hartzfeld PW, Riechel TL. High molecular weight plant polyphenolics (tannins) as biological antioxidants. J. Agric. Food. Chem. 1998; 46:1887–1892.

(31). Pinkerton NM, Grandeury A, Fisch A, Brozio J. r. Riebesehl BU, Prud'homme RK. Formation of Stable Nanocarriers by in Situ Ion Pairing during Block-Copolymer-Directed Rapid Precipitation. Mol. Pharm. 2012; 10:319–328. [PubMed: 23259920]

(32). Ejima H, Richardson JJ, Liang K, Best JP, van Koeverden MP, Such GK, Cui J, Caruso F. One-step assembly of coordination complexes for versatile film and particle engineering. Science. 2013; 341:154–157. [PubMed: 23846899]

(33). Barrett DG, Sileika TS, Messersmith PB. Molecular diversity in phenolic and polyphenolic precursors of tannin-inspired nanocoatings. Chem. Commun. 2014; 50:7265–7268.

(34). Sileika TS, Barrett DG, Zhang R, Lau KHA, Messersmith PB. Colorless Multifunctional Coatings Inspired by Polyphenols Found in Tea, Chocolate, and Wine. Angew. Chem. Int. Ed. 2013; 52:10766–10770.

(35). Wolak MA, Melinger JS, Lane PA, Palilis LC, Landis CA, Delcamp J, Anthony JE, Kafafi ZH. Photophysical properties of dioxolane-substituted pentacene derivatives dispersed in tris (quinolin-8-olato) aluminum (III). J. Phys. Chem. B. 2006; 110:7928–7937. [PubMed: 16610891]

(36). Han J, Zhu Z, Qian H, Wohl AR, Beaman CJ, Hoye TR, Macosko CW. A simple confined impingement jets mixer for flash nanoprecipitation. J. Pharm. Sci. 2012; 101:4018–4023. [PubMed: 22777753]

(37). Lim J, Yeap SP, Che HX, Low SC. Characterization of magnetic nanoparticle by dynamic light scattering. Nanoscale Res. Lett. 2013; 8:1–14. [PubMed: 23279756]

(38). Pansare VJ, Bruzek MJ, Adamson DH, Anthony J, Prud'homme RK. Composite Fluorescent Nanoparticles for Biomedical Imaging. Mol. Imaging. Biol. 2014; 16:180–188. [PubMed: 24129739]

(39). Repetto G, del Peso A, Zurita JL. Neutral red uptake assay for the estimation of cell viability/cytotoxicity. Nat. Protoc. 2008; 3:1125–1131. [PubMed: 18600217]

(40). Wolfe KL, Liu RH. Cellular antioxidant activity (CAA) assay for assessing antioxidants, foods, and dietary supplements. J. Agric. Food. Chem. 2007; 55:8896–8907. [PubMed: 17902627]

(41). Manders E, Verbeek F, Aten J. Measurement of co-localization of objects in dual-colour confocal images. J. Microsc. 1993; 169:375–382.

(42). Zinchuk V, Zinchuk O, Okada T. Quantitative colocalization analysis of multicolor confocal immunofluorescence microscopy images: pushing pixels to explore biological phenomena. Acta Histochem. Cytochem. 2007; 40:101. [PubMed: 17898874]

(43). Schofield P, Mbugua D, Pell A. Analysis of condensed tannins: a review. Anim. Feed Sci. Tech. 2001; 91:21–40.

(44). Ross T, Francis R. The treatment of rusted steel with mimosa tannin. Corros. Sci. 1978; 18:351–361.

(45). Sungur Ş, Uzar A. Investigation of complexes tannic acid and myricetin with Fe (III). Spectrochimic. Acta. 2008; 69:225–229.

(46). Hem, JD. Complexes of Ferrous Iron with Tannic Acid: Chemistry of Iron in Natural Water. 1960.

(47). Johnson BK, Prud'homme RK. Mechanism for rapid self-assembly of block copolymer nanoparticles. Phys. Rev. Lett. 2003; 91:118302. [PubMed: 14525460]

(48). Iglesias J, De Saldaña EG, Jaén J. On the tannic acid interaction with metallic iron. Hyperfine Interact. 2001; 134:109–114.

(49). Rahim AA, Kassim J. Recent development of vegetal tannins in corrosion protection of iron and steel. Recent Pat. Mater. Sci. 2008; 1:223–231.

(50). Spaeth JR, Kevrekidis IG, Panagiotopoulos AZ. Dissipative particle dynamics simulations of polymer-protected nanoparticle self-assembly. J. Chem. Phys. 2011; 135:184903-1–11. [PubMed: 22088077]

(51). Chen T, D'Addio SM, Kennedy MT, Swietlow A, Kevrekidis IG, Panagiotopoulos AZ, Prud'homme RK. Protected peptide nanoparticles: experiments and brownian dynamics simulations of the energetics of assembly. Nano Lett. 2009; 9:2218–2222. [PubMed: 19413305]

(52). Perron NR, Brumaghim JL. A review of the antioxidant mechanisms of polyphenol compounds related to iron binding. Cell Biochem. Biophys. 2009; 53:75–100. [PubMed: 19184542]

(53). Chvátalová K, Slaninova I, Březinová L, Slanina J. Influence of dietary phenolic acids on redox status of iron: Ferrous iron autoxidation and ferric iron reduction. Food Chem. 2008; 106:650–660.

(54). Mannhold R, Poda GI, Ostermann C, Tetko IV. Calculation of molecular lipophilicity: State-of-the-art and comparison of log P methods on more than 96,000 compounds. J. Pharm. Sci. 2009; 98:861–893. [PubMed: 18683876]

(55). Schmaljohann D. Thermo-and pH-responsive polymers in drug delivery. Adv. Drug Deliver. Rev. 2006; 58:1655–1670.

(56). Kumar V, Hong SY, Maciag AE, Saavedra JE, Adamson DH, Prud'homme RK, Keefer LK, Chakrapani H. Stabilization of the nitric oxide (NO) prodrugs and anticancer leads, PABA/NO and double JS-K, through incorporation into PEG-protected nanoparticles. Mol. Pharm. 2009; 7:291–298. [PubMed: 20000791]

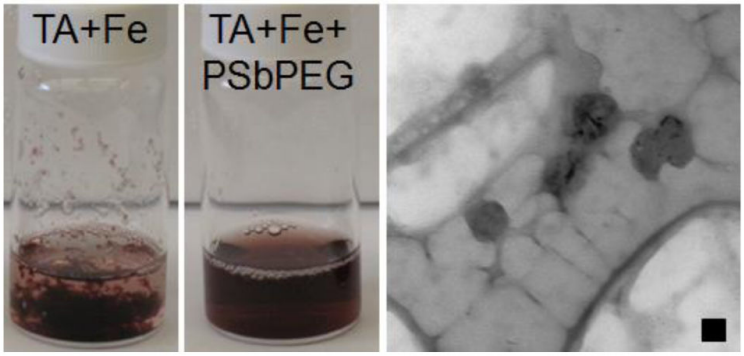

Figure 1.

Tannic acid and iron after rapid mixing without (left) and with (center) a stabilizing amphiphilic block copolymer. Without the block copolymer macroscopic precipitation is observed. A TEM micrograph of the stabilized nanoparticle dispersion is shown on the right with a 50 nm scale bar.

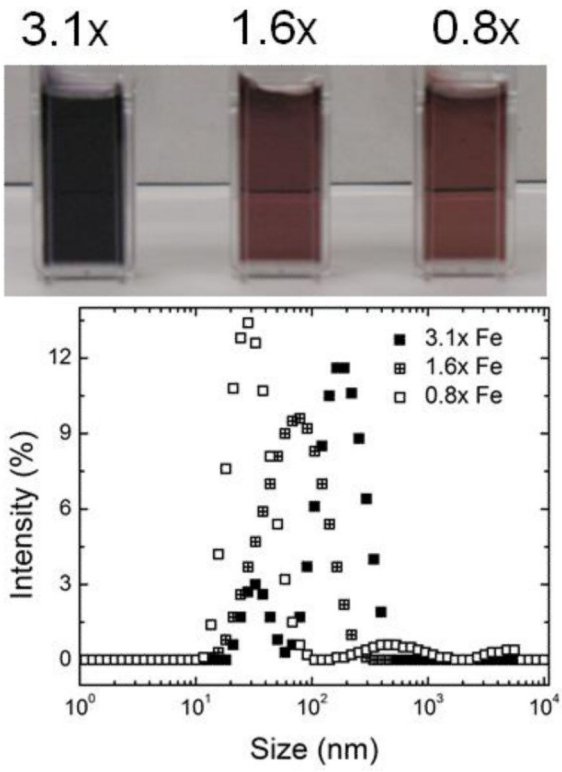

Figure 2.

Effect of iron concentration relative to tannic acid concentration on nanoparticle assembly. In a large excess of iron (3.1 mol excess relative to tannic acid) the dispersion appears purple indicating precipitates of iron and tannic acid and a micelle population is evident in the particle size distribution measured by dynamic light scattering. At lower iron concentrations, the dispersions appear red indicative of a tannic acid iron complex. Particle size decreases with increasing iron concentration.

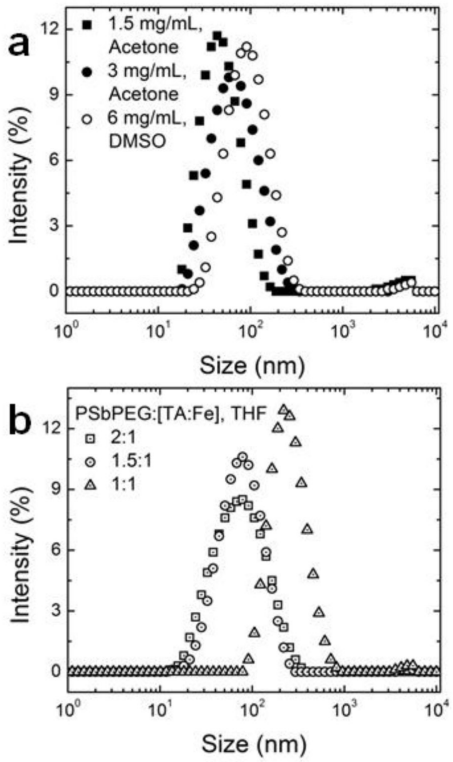

Figure 3.

Tuning nanoparticle size: (a) nanoparticle size increases with increasing total solids concentration and (b) particle size increases with decreasing block copolymer to core material ratio. The ratio of block copolymer to core material ratio is reported in terms of mass (wt.: wt.) and the molar ratio of iron to tannic acid ratio was 1.6:1 mol:mol.

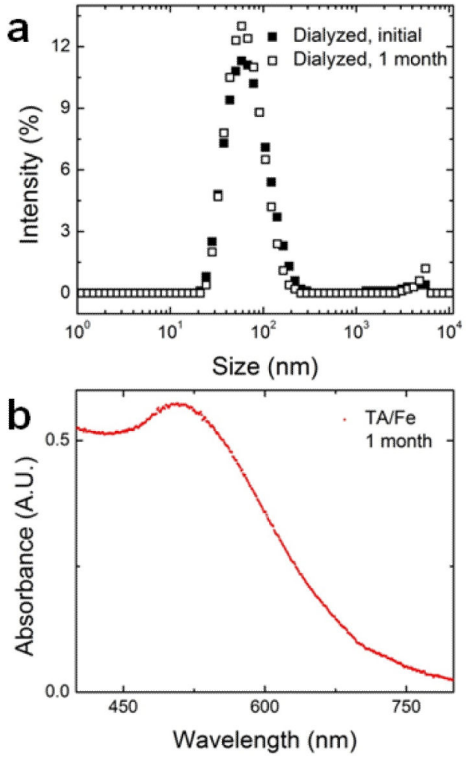

Figure 4.

Particle stability as indicated by (a) no significant change in nanoparticle size or size distribution measured by dynamic light scattering and (b) the initial red color associated with the tris complex of tannic acid and iron is retained over 1 month as indicated by the UV absorbance spectrum (UV maximum absorbance 496 nm). No significant change in the absorbance spectra was observed after 1 month.

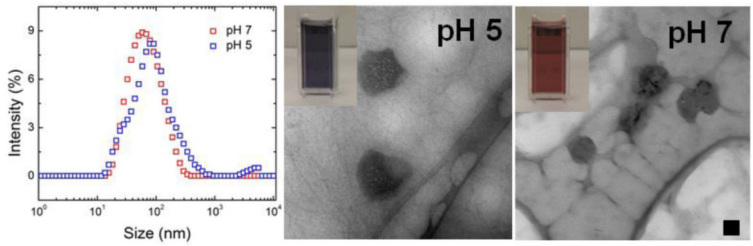

Figure 5.

Particle rearrangement with pH shift. At pH 7.4, dispersions appear red (UV maximum absorbance 496 nm) with a uniform nanoparticle size distribution. TEM indicates single spherical iron containing core. At pH 5, the dispersions appear purple (UV maximum absorbance 561 nm) consistent with the bis-complex of tannic acid and iron. By dynamic light scattering, there is evidence of a shoulder at smaller sizes. The TEM at pH 5 shows evidence of swelling of the cores. Scale bar 50 nm.

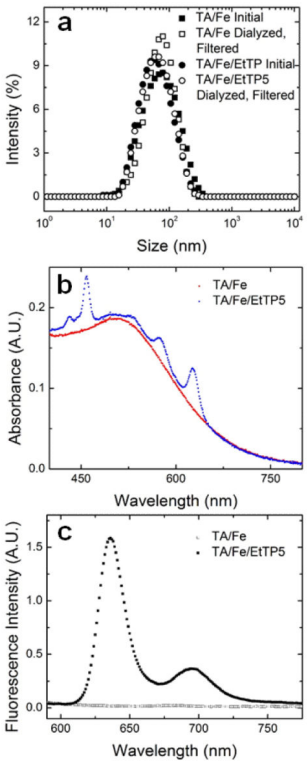

Figure 6.

Characterization of fluorescent tannic acid/iron particles produced by coprecipitating the tannic acid/iron complex with a hydrophobic fluorescent dye, EtTP-5. (a) Coprecipitation with dye does not significantly affect particle size or size distribution measured by dynamic light scattering (b) UV absorbance shows absorbance peaks due to the presence of the EtTP-5 and (c) fluorescence spectra show emission peaks at 635 nm and 695 nm when excited at 460 nm due to presence of EtTP-5.

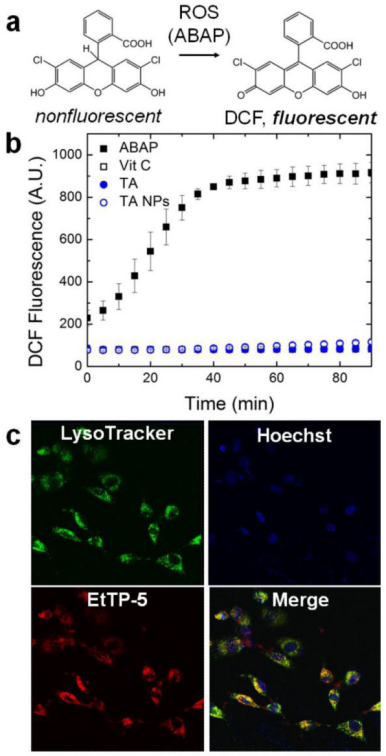

Figure 7.

Intracellular antioxidant activity in 3T3 fibroblasts in vitro (a) intracellularly deacetylated DCFH-DA (DCFH) is converted by reactive oxygen species (ROS) into fluorescent dichlorofluorescein (DCF), the fluorescence of which is measured in the presence of an applied oxidative stress (free radical generator, ABAP), (b) normalized fluorescence of untreated cells with applied oxidative stress compared to cells treated with 50 μg/mL TA, vitamin C or TA NPs, and (c) uptake of EtTP-5 loaded nanoparticles (red) at 1000 μg TA NPs/mL (d = 73.5 ± 1.5 nm) colocalized with the lysosomes stained green (LysoTracker® Green). Antioxidant-loaded nanoparticles prevent oxidative stress induced production of DCF.